

Article

Flash Flood Prediction by Coupling KINEROS2 and HEC-RAS Models for Tropical Regions of Northern Vietnam

Hong Quang Nguyen *, Jan Degener † and Martin Kappas †

GIS & Remote Sensing Section, Institute of Geography, Cartography, Georg-August University
Goettingen, Goldschmidt Street 5, D-37077 Goettingen, Germany;
E-Mails: jdegene@uni-goettingen.de (J.D.); mkappas@gwdg.de (M.K.)

† These authors contributed equally to this work.

* Author to whom correspondence should be addressed;

E-Mail: hong-quang.nguyen@geo.uni-goettingen.de or hongquang116@yahoo.com;

Tel.: +49-551-399805; Fax: +49-551-398020.

Academic Editor: Luca Brocca

Received: 27 August 2015 / Accepted: 11 November 2015 / Published: 17 November 2015

Abstract: Northern Vietnam is a region prone to heavy flash flooding events. These often have devastating effects on the environment, cause economic damage and, in the worst case scenario, cost human lives. As their frequency and severity are likely to increase in the future, procedures have to be established to cope with this threat. As the prediction of potential flash floods represents one crucial element in this circumstance, we will present an approach that combines the two models KINEROS2 and HEC-RAS in order to accurately predict their occurrence. We used a documented event on 23 June 2011 in the Nam Khat and the larger adjacent Nam Kim watershed to calibrate the coupled model approach. Afterward, we evaluated the performance of the coupled models in predicting flow velocity (FV), water levels (WL), discharge (Q) and streamflow power (P) during the 3–5 days following the event, using two different precipitation datasets from the global spectral model (GSM) and the high resolution model (HRM). Our results show that the estimated Q and WL closely matched observed data with a Nash–Sutcliffe simulation efficiency coefficient (NSE) of around 0.93 and a coefficient of determination (R^2) at above 0.96. The resulting analyses reveal strong relationships between river geometry and FV, WL and P. Although there were some minor errors in forecast results, the model-predicted Q and WL corresponded well to the gauged data.

Keywords: flash flood; prediction; KINEROS2; HEC-RAS; modeling; tropics; discharge; flow velocity; flood stage

1. Introduction

Unlike paleoflood, flash floods (FF) occur in small streams [1] and are linked to short, but extreme rainfall events [2]. However, they have been categorized into fatal and costly natural disasters [3–5]. Northern Vietnam is one of the regions most affected by FF in Vietnam and likely to suffer more frequently due to the impacts of climate change [6]. Thus, there exists an urgent requirement for FF-related studies. Much previous research has suggested approaches to mitigate the impacts of FFs through the early identification of FF occurrences (time and location) or their forecast [7–12]. This is crucial information for the local people, as such information will help them to protect themselves from these floods [13]. In this study, we modelled and predicted the occurrence of a specific FF event that took place on 23 June 2011 in the Nam Khat watershed and extended the modelling to the adjacent watershed of Nam Kim, Yen Bai province, Vietnam. This work was done by coupling the KINEROS2 (kinematic runoff and erosion) and HEC-RAS (the Hydraulic Engineering Center River Analysis System) models employing satellite-based and forecast rainfall.

Numerous attempts have been made to forecast FF occurrence using modeling approaches for different conditions of complex terrain [10,14–16], urban and rural areas [15,17], ungauged zones [18–20] or in the tropics [7,21]. Other studies have taken advantage of the finer resolution of radar rainfall and operated in real or near real time [5,22–24], though several other options exist using satellite-derived precipitation data [25,26]. Defining FF is difficult [12]. However, an FF is recognized by its physical characteristics of massive power (energy), fast flows (velocity) [5,12] and high discharge stage (water level) [27]. In our modeling implementations, we focused more on these physical characteristics (not the social impacts) of FFs and predicted them based on forecast rainfall inputs. When FFs are identified at an early stage, this information is extremely helpful for flash flooding warning systems [28].

Prior warning of FFs is very complicated, not only because of the complexity of the system (physical processes, short leading time), but also the output uncertainty (related to scant available data, methodology) [29–31]. Therefore, many researchers have attempted to analyze the uncertainty sources [9,32,33]. One major issue in early FF research concerned the forecast uncertainty and its significant dependence on meteorological inputs (rainfall) [23]. Our result accuracy relied on the merit of two robust models and validated observed data utilizing the method by Nash and Sutcliffe [34].

The aim of this study is to use the two well-known hydrological models, firstly, for calibrating and validating the models and making sure that the models work properly; secondly, for modeling the past flooding event and analyzing the hydraulic response by looking at river discharge, flow velocity and power and their relationships; thirdly, for running the models in forecast mode using forecast rainfall data and comparing the model outputs with observed information. In the forecast

stage, the three important aspects of flow stage, flow velocity (FV) and streamflow force were analyzed, as well.

To achieve the study goals, we designed a practical framework with a combination of the well-known robust models (in terms of precision and computational efficiency). The benefit of coupling the two models is to solve the data scarcity problem when the finer input data required by the HEC-RAS were not available. In addition, there have been some studies using the KINEROS2 model alone for the aim of FF prediction [16,33,35,36] that recommended the use of it; however, the KINEROS2 does not accurately estimate the river water level and flow force (two important criteria for identifying the FF), but the use of HEC-RAS afterwards could be a good solution. As the FFs often occur within six hours of causative rains [37] or a shorter event of a few hours [38], the total model operation time (including preparing new model inputs, model runs and the result display and analyses) should meet this time criterion. Otherwise, the information provided by the model for FF warning might be too late for the warning system in a real-time operation. With an Intel core™ i3, 2 GB RAM computer, the models need less than one minute to run the modelling of the bigger watershed of Nam Kim (268.5 km²). Only new updated forecast rainfall and input discharge for HEC-RAS are needed to re-input for forecast operation. The time for preparing these inputs is assumed to depend on the skill of the operators, and for this study, approximately 30 min were needed. We recommend seasonal updating for land use and land cover for KINEROS2, and the less dynamic parameters of topography, river and soil profiles could be renewed in a few decades if significant changes are found.

2. Study Site

This study focuses on the region of North Vietnam, which has tropical climatic conditions, steep terrain and an increase in intensive land use [39,40]. The region is considered to have a scarcity of data available, with 108 metrological gauges in the whole region and just three gauges in Yen Bai province. The north of Vietnam has an annual average rainfall ranging from 800 to 1500 mm and annual mean temperature varying from 20 °C to 24 °C [6]. Nam Kim and Nam Khat, located in the red ellipse (Figure 1) within Yen Bai province, were chosen as the representative watersheds of the region.

Both Nam Kim and Nam Khat are classified as medium-sized watersheds. The elected reaches (in the green circles) for HEC-RAS simulation have no construction along them, such as bridges, embankments or dams. Local people cross the rivers on foot or on footbridges (illustrated in Figure 2). Dominant local residents are Tay and Dao ethnicities and are considered to be very vulnerable to flash floods. Nam Kim was chosen for the case study because observational data were available (recorded at the outlet) for model validation and has also experienced some kind of FF, but not severe. Nam Khat was additionally selected due to its flash flooding incidence on 23 June 2011, when four lives were lost (the reach in the green circle in Nam Khat in Figure 1).

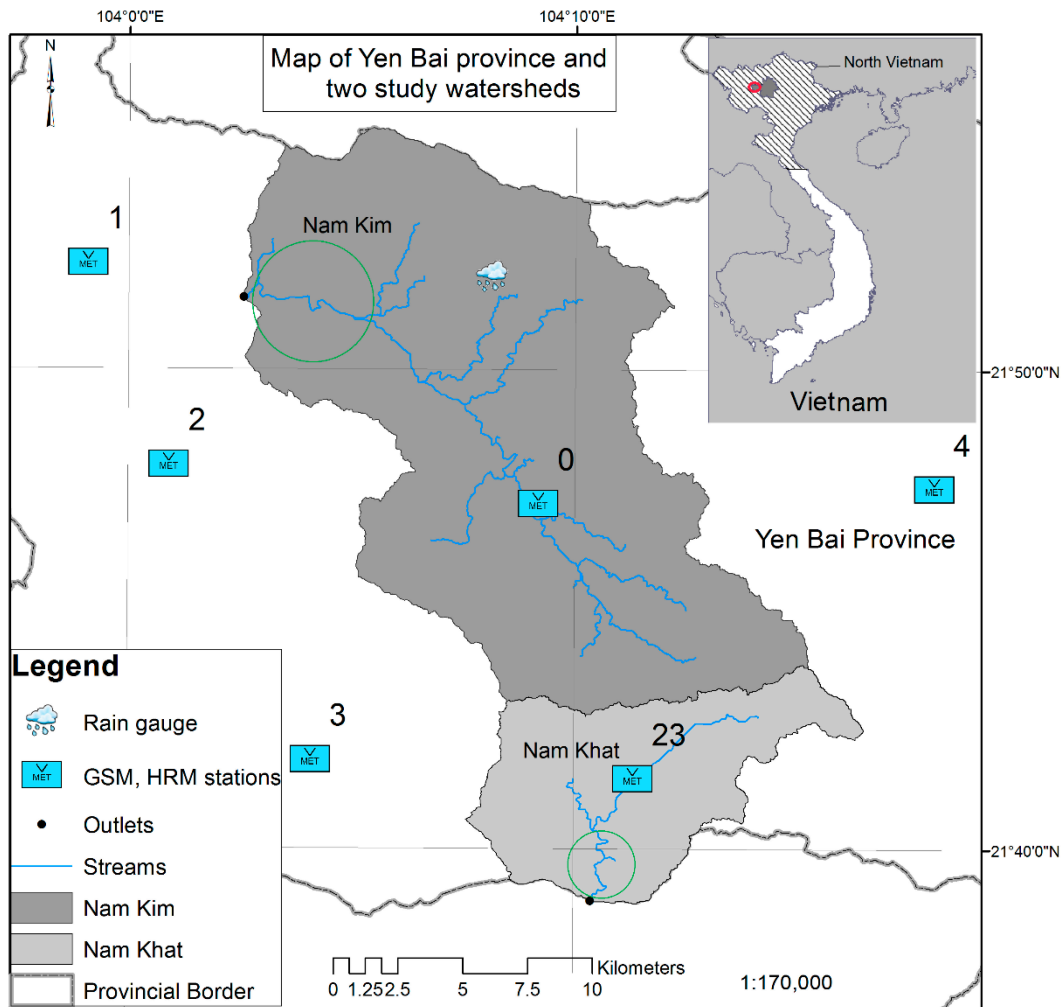


Figure 1. Study site of the Nam Kim and Nam Khat watersheds. GSM, global spectral model; HRM, high resolution model.



Figure 2. Pupils crossing the river on their way to the school (a) and a typical footbridge (b) in rural areas in Vietnam (source: <http://tuyensinh.nld.com.vn> and <http://kienthuc.net.vn>, respectively).

3. Methodology and Materials

3.1. Study Flow Chart

The study framework was designed to accomplish the study objective, as shown in Figure 3. It is important to note that the forecast rainfall by means of the KNIEROS2 model [41,42] will produce the forecast river hydrographs, depth and initial flow, which will be used as inputs for the HEC-RAS and generate the forecast water levels or stages (WLs), flow velocity (FV) and energy curves for the FF forecast strategy.

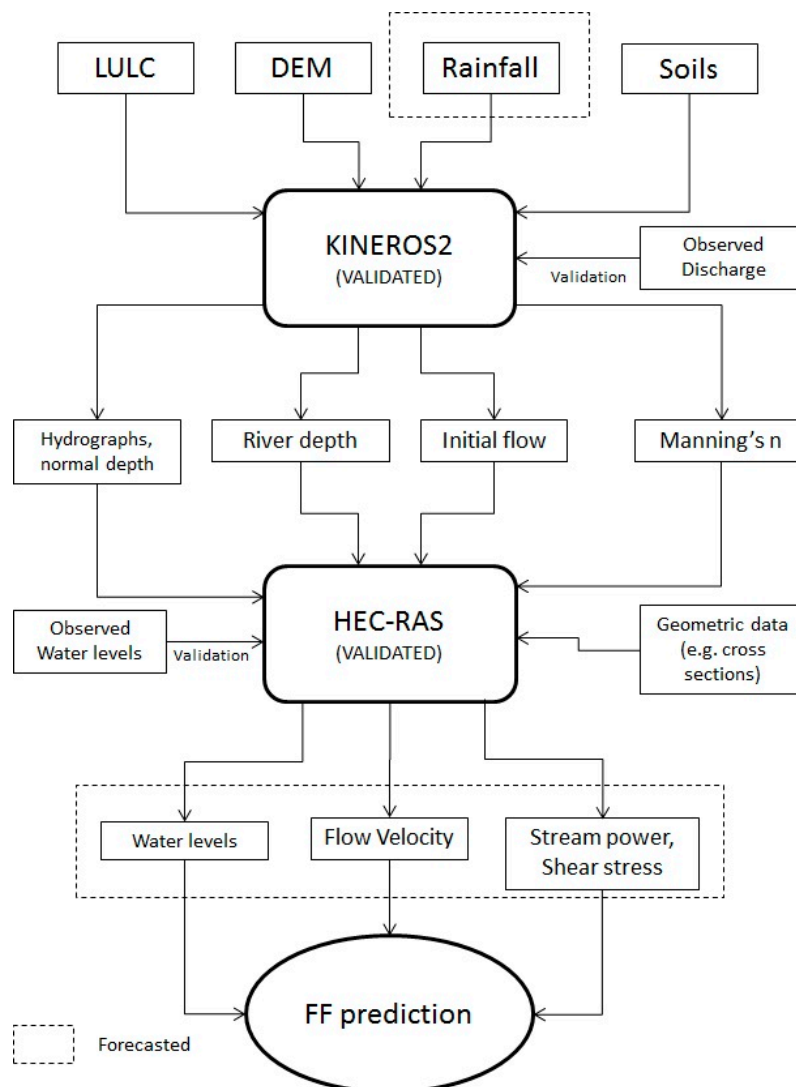


Figure 3. The study flow chart. FF, flash flood.

3.2. Model Description

3.2.1. KINEROS2

KINEROS2 is the improved version of KINEROS [43] and a dynamic, distributed simulation model. Most model features were written by Smith *et al.* [41]. The model requires four types of

datasets to operate, namely topographic, rainfall, soil and land use data. Some of the useful features for the later HEC-RAS inputs will be presented as follows.

KINEROS2 treats the channel routine discharge (Q) using a four-point implicit technique. Manning’s roughness coefficient can be retreated in the kinematic wave approximation equation (for more details, see [43]).

The hydraulic depth is estimated in KINEROS2 by approximating the channel cross-sections as trapezoidal or circular, as shown in Figure 4 and in the flowing equation:

$$h_D = D \left[\frac{\theta_c - \sin \theta_c}{\sin(\theta_c/2)} \right] / 8 \tag{1}$$

where h_D presents the hydraulic depth (m) and D is the diameter of the channel conduit.

When the channel cross-section is approximated as trapezoidal, the depth is calculated as in the following relationship:

$$p_e = \min \left[\frac{h}{0.15\sqrt{BW}}, 1.0 \right] \times p \tag{2}$$

where h is the depth, p_e presents the effective wetted perimeter for infiltration, p indicates the channel wetted perimeter at depth h and BW is the channel bottom width, as in Figure 4. Equation (2) indicates that the p_e is smaller than the p until a threshold depth is reached, and at depths greater than the threshold depth, the two values are identical.

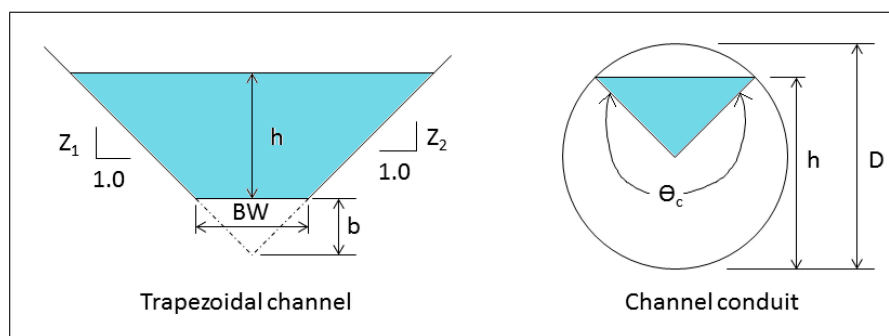


Figure 4. Channel and conduit cross-sections.

3.2.2. The HEC-RAS

The U.S. Army Corps of Engineers’ River Analysis System (HEC-RAS) is software that allows users to perform one-dimensional steady and unsteady flow river hydraulics calculations [44]. In this study, the latter method was applied. The equations of one-dimensional steady and unsteady flow are described by [45]. The following features are the main relationships that are important for FF identification.

The model estimates the channel depth in unsteady flow based on momentum equations expressed by Newton’s second law as in the flowing expression:

$$\sum F_x = \frac{d\vec{M}}{dt} \tag{3}$$

where $\sum F_x$ is the accumulative momentum applied in the x-direction, $d\vec{M}$ indicates the momentum flux, which is the velocity vector in the flow direction, and dt presents the fluid mass times. The pressure, gravity and boundary drag are considered as three forces.

The channel depth can be inferred from the pressure force equation [46]:

$$F_p = \int_0^h \rho g(h - y) T(y) dy \quad (4)$$

where F_p is the pressure force in the x-direction, h is the depth, y is the distance above the channel invert and $T(y)$ presents the width function, which links the width of the cross-section to the distance above the channel invert (for more details, see [44]).

The FV at the discrete cross-section is computed in the HEC-RAS by solving the continuity, energy and flow resistance equation [47]:

$$Y_2 + Z_2 + \frac{\alpha_2 V_2^2}{2g} = Y_1 + Z_1 + \frac{\alpha_1 V_1^2}{2g} + h_e \quad (5)$$

in which Y is water depth, Z indicates channel elevation, V represents the mean velocity, α is a velocity weighting coefficient, g is the gravitational acceleration, h_e represents energy head loss and subscripts 1 and 2 signify Cross-sections 1 and 2, respectively.

To achieve the above outputs, the river geometric, unsteady flow data (boundary and initial conditions) have to be supplied. The boundary condition includes a stage/flow hydrograph (or both) and normal depth derived from KINEROS2.

3.3. Coupling of KINEROS2 and HEC-RAS

We coupled the KINEROS2 and the HEC-RAS models by using the KINEROS2 outputs for the HEC-RAS inputs; however, internally, the two models were performed separately. The discharges (using satellite-based, gauged and forecasted rainfalls), river depths, initial flow and Manning's n coefficient were used for the inputs and for defining the initial conditions in the HEC-RAS, as well. All of these KINEROS2 parameters were derived from the validated calibration stage, and they are, hence, realizable. We applied the unsteady flow analysis approach.

3.4. Calibration and Validation for KINEROS2 and HEC-RAS

KINEROS2 and HEC-RAS calibrations for Nam Kim were made for the rain event on 23 June 2011 (R23rd) using observed discharge and water levels from each model respectively. In these stages, the hydraulic conductivity (K_{sat}) and relative saturation index (S) were adjusted for the KINEROS2, and Manning's n coefficient (N) was altered for the HEC-RAS calibration.

Other rain events on 30 June (R30th), 8 (R8th) and 31 (R31st) July 2011 were elected for model validations employing field measurements of the hydraulic gauge at the Nam Kim outlet. The implementations of the models were investigated by using statistical values of the Nash–Sutcliffe simulation efficiency coefficient (NSE) [34], the coefficient of determination (R^2) and graphical approaches of comparing simulated with observed information. Unfortunately, there was no gauged data recorded for the validation in Nam Khat. However, due to the similar conditions of the two

watersheds, the model calibration for Nam Kim could be transposed to the ungauged Nam Khat, a method that has been applied in several studies, such as [8,18,20,48].

3.5. Data for KINEROS2

3.5.1. Rainfall

Precipitation data were derived from three sources of satellite-based (MSAT-Japan), ground rain gauges and the Numerical Weather Prediction (NWP) models of the global spectral model (GSM) [49] and the high resolution model (HRM) [50]. All of this rainfall data were supplied by the National Center for Hydro-Meteorological Forecasting, Vietnam.

The temporal and spatial resolutions of the satellite-based rainfall are 30 min and 4 km × 4 km, respectively. The accumulative distributed rainfall (the maps in Figure 5) and the 30-min rain density (the graphs in Figure 5) of the R23rd and R30th were assessed for Nam Kim and Nam Khat.

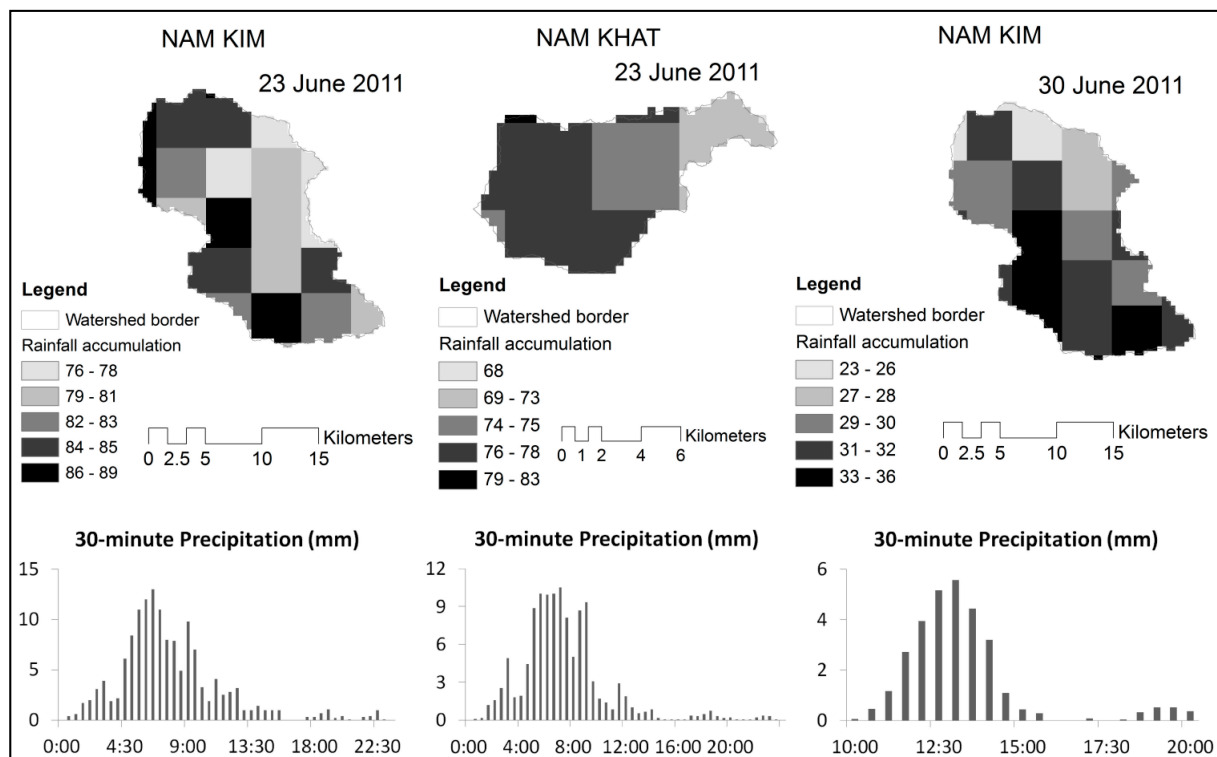


Figure 5. Satellite-based rainfall.

We also used gauged rainfall recorded every three hours on 8 July (R8th) and 30 to 31 (R31st) July 2011 by the rain gauge established at Nam Kim (Figure 1) for validations of the models. The development of the rain is represented in the section 4.1.1.

The 6-h, accumulated rainfall of GSM (84-h forecast) and HRM (132-h forecast) was the forecasted observation at 00:00 on 23 June 2011 (Figure 6) at Stations 0 and 23 (locations shown in the study site figure). Both of the models have the ability to operate at large, meso- and small (grid) scales and take about 50 min for each operation. The GSM was operating four times a day at 00:00, 06:00, 08:00 and 12:00, and the HRM was operating at 00:00 and at 12:00.

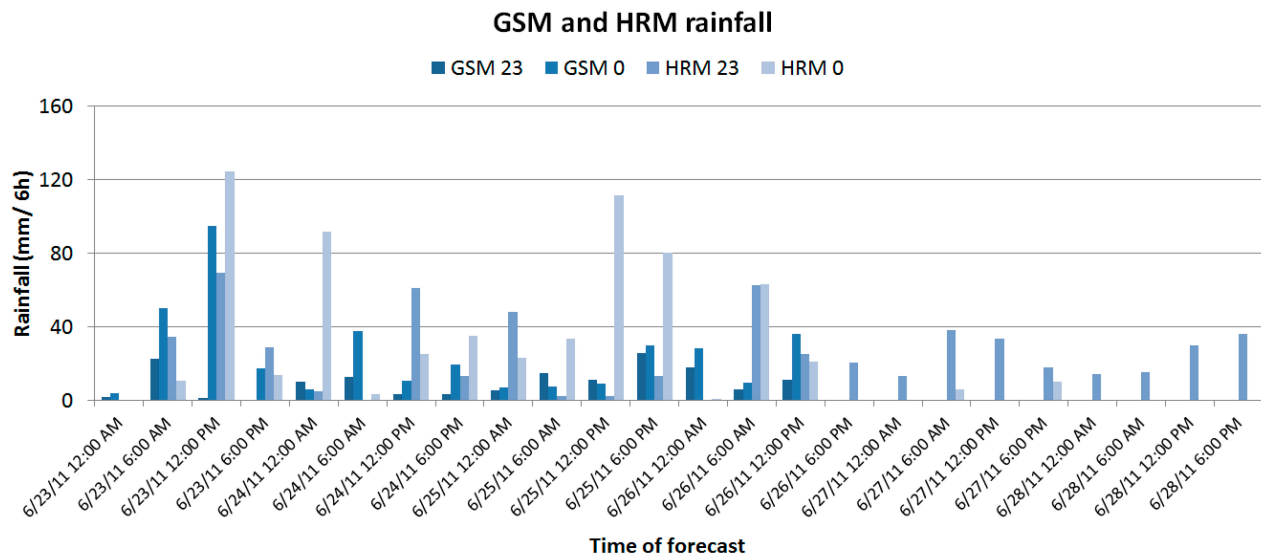


Figure 6. Forecasted rainfall by the GSM and the HRM of the designed stations 23 and 0.

3.5.2. Land Use, Digital Elevation Model, Soil and Discharge Data

The LULC map was mapped from the Landsat scene with a 30×30 meter spatial resolution acquired in 2009. The forest, shrub, agricultural land, grassland, water bodies and bare land are classified as the six major land uses. The accuracy of the LULC map was examined using the producer accuracy (76.5%), user accuracy (76.7%) and kappa statistics (0.74), as well.

A $10 \text{ m} \times 10 \text{ m}$ grid-based DEM was used for the KINEROS2 morphologic parameterizations. It was provided by the Vietnam Resources and Environment Corporation in 2009.

The dominant soil groups of Fluvisols, Calcisols, Ferralsols, Alisols, Acrisols and Gleysols were categorized on a custom soil map and employed as soil data for the model. The map was produced by the Resource Centre-Agricultural Institute of Plan and Design, Vietnam in 1996 [51].

Finally, we employed the hourly discharge and WLs measured at the outlet of Nam Kim provided by National Centre for Hydro-Meteorological Forecasting (NCHMF) [52] for the calibration and validation of the two models.

3.6. Data for HEC-RAS

3.6.1. Geometric Data

River cross-sections (RS) were built at points (up to 50 meters above the river banks), which were directly measured on the Aerial Photogrammetry Station of the Intergraph Corporation, USA, with absolute geometric errors of less than one meter. The river depths were derived from the KINEROS2 results. We used the trapezoidal channel to define the channel shape. The Nam Kim reach (Table 1) (3.5 km) was defined by sixteen RSs and Nam Khat (Table 2) (1.2 km) by twelve RSs. The distance between cross-sections is chosen based on the changes in river slope. The elevation of the river banks was derived from a geodatabase of Yen Bai province, and these banks were *in situ* field measurements.

Table 1. Geometric profiles of the Nam Kim reach (Chl = channel; W.S. = water surface; E.G. = energy grade line for the calculated W.S.).

River Stations	Min Chl Elevation (m)	W.S. Elevation (m)	E.G. Elevation (m)	E.G. Slope (m/m)	Flow Area (m ²)	Top Width (m)
101	904.2	907.0	907.4	0.0014	121.3	53.3
102	903.4	906.0	906.9	0.0043	85.4	53.6
103	901.0	903.9	906.1	0.0089	54.0	31.2
104	899.3	903.4	903.7	0.0007	155.0	56.3
105	899.5	902.8	903.4	0.0021	90.1	34.7
106	898.8	901.9	903.0	0.0040	67.9	26.4
107	899.3	901.7	902.2	0.0022	101.4	46.8
108	898.5	900.6	901.9	0.0075	67.8	44.3
109	896.9	899.2	900.3	0.0053	70.5	38.4
110	896.0	897.8	898.7	0.0066	76.3	52.7
111	893.8	896.3	899.6	0.0188	51.3	39.9
112	890.7	892.4	893.9	0.0109	57.8	37.5
113	888.0	889.5	891.8	0.0269	46.8	45.1
114	880.6	883.5	884.6	0.0044	69.2	30.6
115	880.4	882.6	883.3	0.0039	83.9	45.0
116	879.0	882.7	882.9	0.0004	195.6	61.0

Table 2. Geometric profiles of the Nam Khat reach.

River Stations	Min Chl Elevation (m)	W.S. Elevation (m)	E.G. Elevation (m)	E.G. Slope (m/m)	Flow Area (m ²)	Top Width (m)
101	1250.5	1252.5	1253.1	0.0184	62.2	34.7
102	1247.2	1249.5	1250.0	0.0229	65.0	44.2
103	1245.4	1246.8	1247.6	0.0239	54.6	42.1
104	1239.3	1243.2	1244.1	0.0186	53.1	20.3
105	1236.9	1240.2	1241.0	0.0173	63.6	36.3
106	1235.1	1237.9	1238.4	0.0194	70.3	36.0
107	1233.9	1236.0	1236.6	0.0152	67.9	48.6
108	1228.1	1232.7	1233.4	0.0189	66.9	24.0
109	1226.2	1230.5	1231.2	0.0136	68.7	26.2
110	1223.8	1228.0	1229.2	0.0198	50.5	18.6
111	1220.1	1224.1	1225.3	0.0164	46.9	16.8
112	1216.0	1220.1	1220.8	0.0126	63.7	28.4

3.6.2. On-Site Measured River Discharge and Water Levels

Hourly (two-hour recordings for the cases of R8th and R31st) discharge and river stages were recorded during the R23rd, R30th, R8th and R31st at the outlet of the Nam Kim River by the NCHMF [52]. These data were used for the calibrations and validations of the models (see the study flow chart).

3.7. Regionalization Technique

We used the regionalization technique, defined as a method of transferring model parameters from calibrated catchments to ungauged ones of similar characteristics [53], for Nam Khat. The two watersheds are neighbors (Figure 1) and located in the same climatic zone [6]. The Humic Ferralsols and Humic Acrisols are both major soils in the watersheds. LULC is also similar to the major classes of forest, shrub and agricultural land, and both watersheds have complex and mountainous terrain (statistics from the inputs).

4. Results and Discussion

To accomplish the study objective of flash flood prediction, the FV, the WLs and the flow energy (all related to peak discharge) are considered to be influential with respect to FF occurrence [9,54,55]. KINEROS2 was calibrated and validated, and the outputs were used for HEC-RAS. Next, we investigated the capacity of the HEC-RAS model to accurately estimate these factors. Then, we applied the model for the prediction stage by using forecasted discharge from KINEROS2. HEC-RAS also offers a module to map the flooding plains. However, due to the very steep riverbanks of the study areas, the flooding areas are of less importance to our study compared to the factors mentioned above.

4.1. Model Calibration and Validation

4.1.1. KINEROS2

The results of KINEROS2 calibration for the R23rd in the Nam Kim watershed can be seen as represented by the hydrographs in Figure 7a as a result of changing the most sensitive parameters of the saturation index of the soil (initial value of 0.2 and final value of 0.46) and the Ksat (average initial value of 5.16 and final value of 4.12). Additionally, the Nash–Sutcliffe simulation efficiency (NSE) and coefficient of determination (R^2) were above 0.95 comparing the observed data with the discharge calibrated after.

The model appeared very stable in the validation stage, with the R30th illustrating great accuracy ($R^2 = 0.97$ and $NSE = 0.91$) in Figure 7b. A slightly reduction of agreement between simulated and observed discharges has been found in the validation for gauged rains on 8 July 2011 with R^2 of 0.90 and NSE of 0.89 and on 30–31 July 2011 with R^2 of 0.79 and NSE of 0.71 (Figure 7c,d). This accurate reduction could be a result of different rain types (satellite and gauged) being used and the variation of rain intensity, as well. In general, although there was a different temporal resolution of the simulated (a minute) and recorded (an hour) data, graphically, they matched each other well.

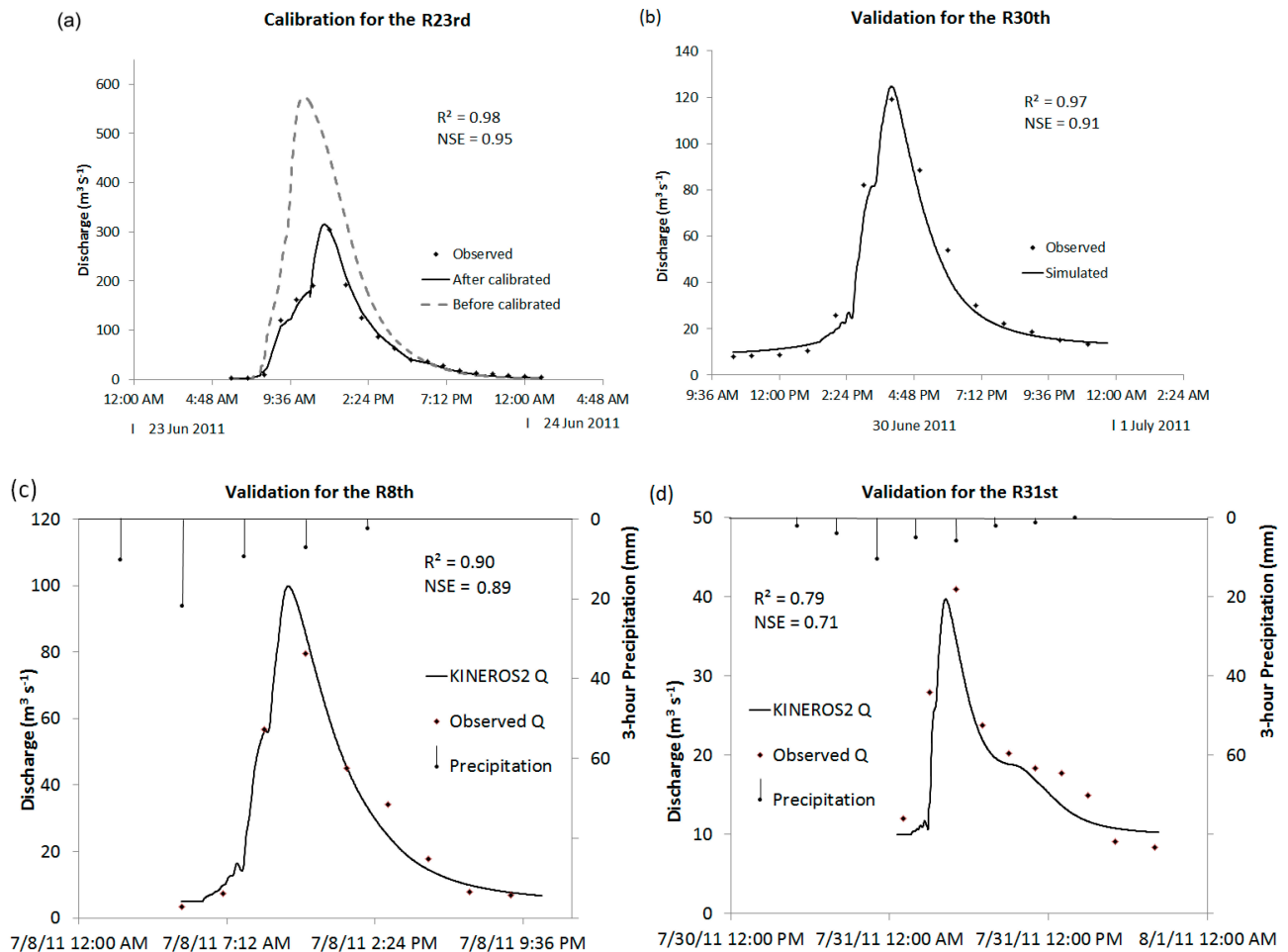


Figure 7. The KINEROS2 results of calibration and validation. (a) for the rain event on 23 June; (b) on 30 June; (c) on 8 July; and (d) on 31 July 2011.

4.1.2. HEC-RAS

What is interesting in the calibration hydrographs shown in Figure 8a is that in the simulation phase, there was an overestimate of WL compared to the field measured data. However, the time of the peak was accurately computed. On the other hand, according to after the calibration, they match the observed information almost perfectly. However, the calibrated stage was still lower by the end of the day.

Less accurate simulation was found in the validation for the R30th with the R^2 of 0.96 and NSE of 0.92 compared to the R^2 of 0.97 and NSE of 0.94 in the model calibration. A similar scenario of water levels predicted by the HEC-RAS also can be seen in Figure 8c,d, with a slight decrease of both the R^2 and NSE. In addition, the model might overestimate the peaks of water levels, or this could be a result of the difference in the temporal resolution of the estimated and observed WL. Otherwise, this performance was affirmed to be a fine implementation. This dependence has also been shown in several other study results [56–58].

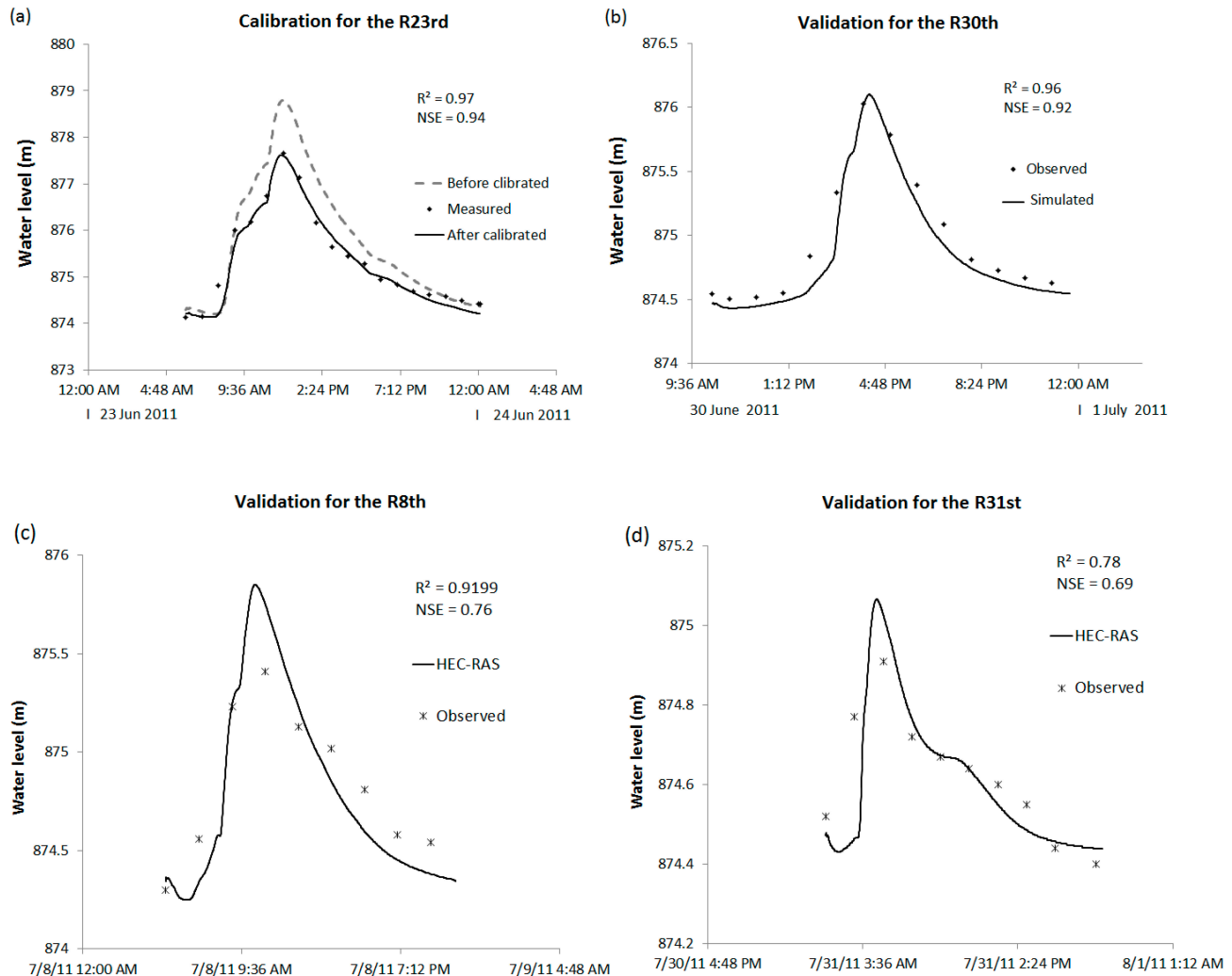


Figure 8. Results of calibration and validation for HEC-RAS. (a,b) using satellite-based rainfall; (c,d) using gauged rainfall.

4.2. Relationship between HEC-RAS Discharge and Water Level

Correlations between flow value and water level were modelled at the outlets (RS101) and upstream RSs (116 and 112) for the R23rd in the Nam Kim and Nam Khat reaches and the R30th in just Nam Kim (no significance was found in Nam Khat). Graphically, strong relationships are shown in Figure 9 for all of the RSs and the rains (all R^2 are greater than 0.9). Originally, the simulation time interval was one minute, but the rating curves were sustained for up to one hour (the lozenges and crosses) for the graphic presentation with the trends and their equations added. The outstanding ratings were the highest values of flow and stage (the peaks) compared to the elevation of the banks (the red dotted lines). Important riverbank overflows of the R23rd were found in both rivers. On the other hand, the R30th made no serious warning at the upper RS115 of Nam Kim and just a 0.5-meter riverbank overflow of the water level at the outlet (RS101). The accurate estimated peaks of discharge water level are considered to be very important for determining the occurrences of FFs [59–61] and, as such, helpful for FF warning systems [62]. Furthermore, Carpenter *et al.* [63] asserted that FFs likely happen when the river discharge (directly related to WL and FV) slightly exceed flow thresholds. They also

introduced the method to calculate FF runoff thresholds on a national scale using GIS, and similar work was done by Kourgialas *et al.* [38].

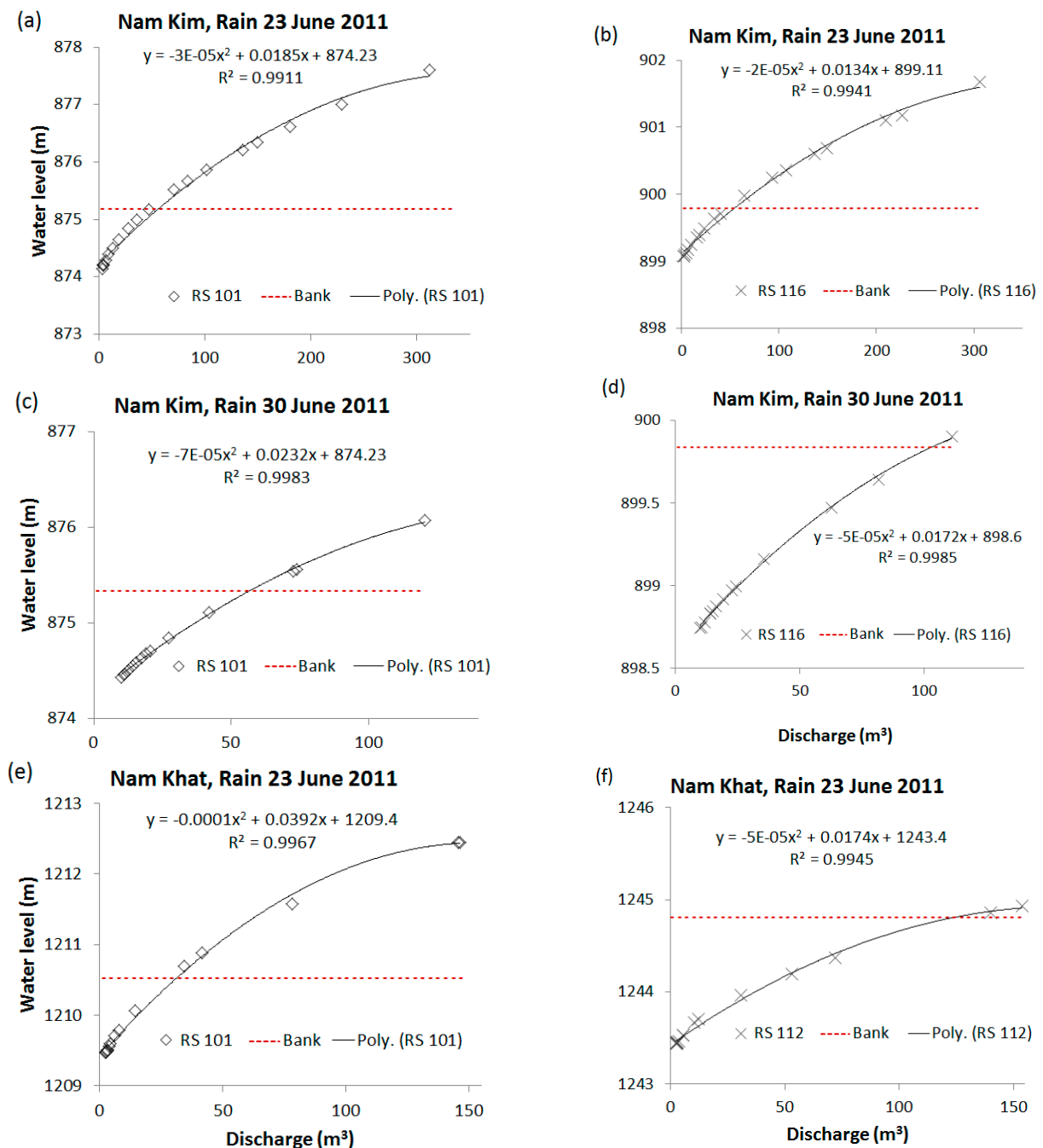


Figure 9. Modelled rating curves compared to river banks. (a) for Nam Kim, the rain event on 23 June at RS 101; (b) at 116; (c) on 30 June 2011 at RS 101; (d) at 116; (e) for Nam Khat, the rain event on 23 June 2011 at RS 101; and (f) at 112. RS, river cross-section.

4.3. Relationship between HEC-RAS Flow Velocity, Channel Slope and Top Width

Figure 10a,b indicates a positive correlation (positive slope of the equations) between modelled-max FV flowing through 16 and 12 RSs of Nam Kim and Nam Khat, respectively, for the R23rd with their slope gradients. It was indicated that the velocity varied widely ranging from 1.8 to 8 m·s⁻¹ in Nam

Kim and from 3.1 to 4.8 m·s⁻¹ in the Nam Khat reach. However, FV is not only dependent on slope [4,27], but also on top width, flow area and discharge, as well. For example, the RS of Nam Kim, which had the biggest slope value, did not produce the highest FV, whereas the second biggest slope gradient did (Figure 10a).

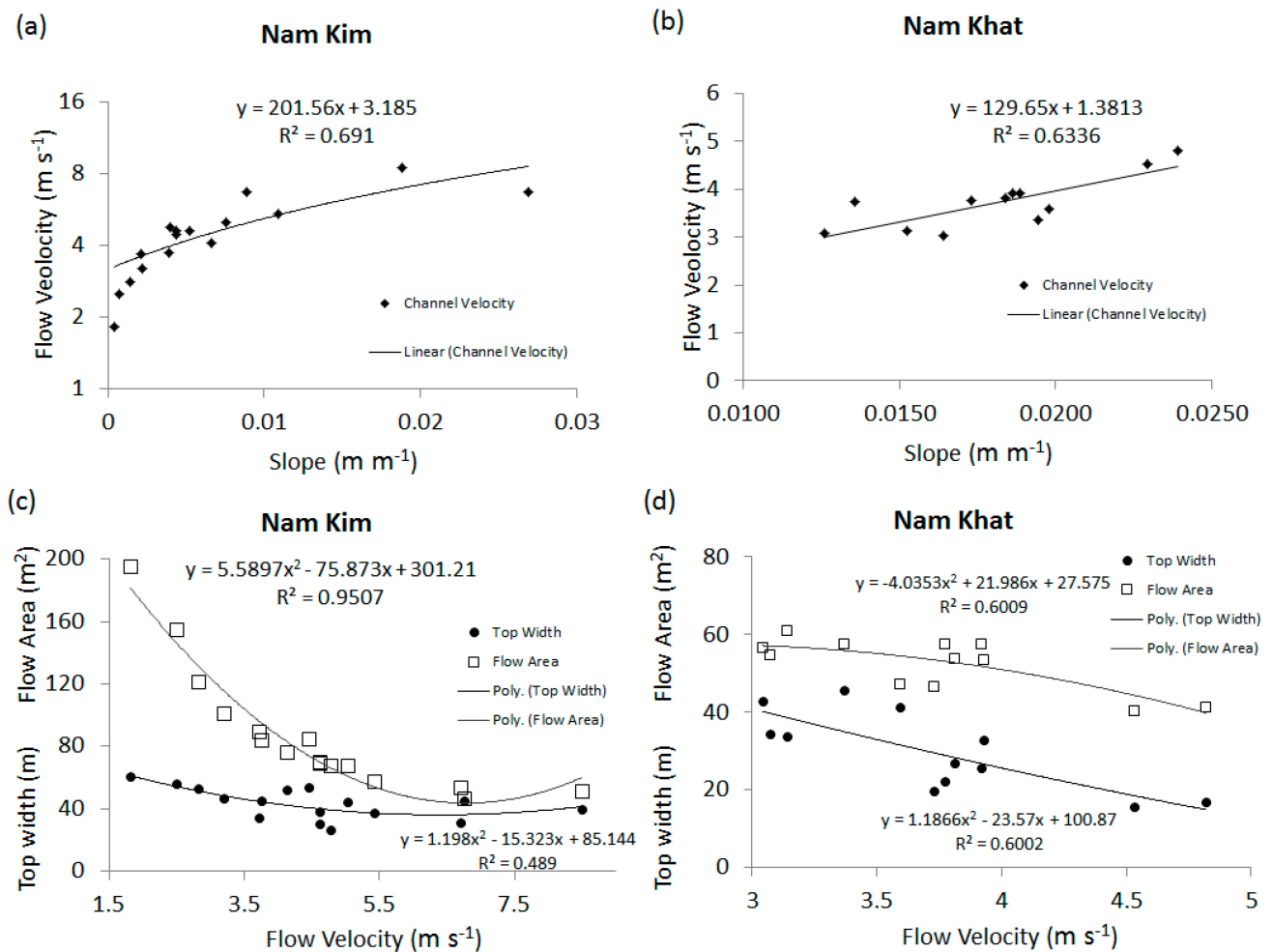


Figure 10. Modelled flow velocity (FV) for the rain event of 23 June 2011 (R23rd) compared to. (a) channel slope of Nam Kim; (b) of Nam Khat; (c) top width and flow area of Nam Kim; and (d) of Nam Khat.

On the other hand, Figure 10c,d represents an inverse proportion of FV to the river top and flow area. In addition, it appeared that the bigger and longer reach of Nam Kim had a stronger relationship ($R^2 = 0.95$) than the smaller and shorter one of Nam Khat ($R^2 = 0.6$). In fact, the total flow area is calculated from the top width and the river depth (according to [44]), and thus, although the trends (the Polys of the Figure 10c,d) were similar, the FL was also driven by the river depth input using the KINEROS2 results. The better the estimated river depth by KINEROS2, the better the FV simulated by HEC-RAS would be. Altogether, the estimated FV had a close relationship to the slope, shape and roughness [54]. This factor is believed to be important for identifying the FF [55,64].

4.4. HEC-RAS Modelling Stream Power and Shear Stress Compared to FV

The total power of the flow, shear stress and average channel velocity values at RSs of the reaches (Table 3) was computed for the R23rd (133 mm of rain accumulation). The flooding event on 23 June 2011 in Nam Khat appeared to be a devastating FF with a great force of around $2000 \text{ N}\cdot\text{m}^{-1}\cdot\text{s}^{-1}$ and shear stress of $530 \text{ N}\cdot\text{m}^{-2}$, particularly at RS102, 103 and 110. On the other hand, although the R23rd (144 mm of rain accumulation) in Nam Kim was a little heavier than in Nam Khat, the flow was much less violent. This trend could be explained by the linkage of the channel slope factor to flow power [65] (Nam Khat had larger slopes than Nam Kim; see Tables 1 and 2 and Figure 10a,b). Additionally, based on Newton's second law of motion and the shear Reynolds number (presented in [44]), the streamflow and shearing forces also have a positive correlation with the channel and friction slope.

The FV distinguishes FFs from other kinds of inundation floods based on the short leading time and its spatial scale (a small scale as compared to paleoflood) [5,59,60], and this is directly linked to slope, as well. The maximum FVs on the channel water surface were considered to be very high, around $8.5 \text{ m}\cdot\text{s}^{-1}$ at RS106 of Nam Kim and $4.8 \text{ m}\cdot\text{s}^{-1}$ at RS103 of Nam Khat. However, in ungauged regions, FFs might be recognized through our realization, for example the WL and FV in Nam Kim (also see the discussion above) were higher than in Nam Khat, but no FF was identified, because no lives and property were lost there due to this event. The important information in Table 3 is the overview of the FV and forces distributions within the reaches of Nam Kim and Nam Khat, as they are assumed to be useful for identifying the location of FFs, as well as their degree of danger.

Table 3. Estimated total flow power, shear stress and average channel FV for Nam Kim and Nam Khat.

Watershed\RS	101	102	103	104	105	106	107	108	109	110	111	112	113	114	115	116
Nam Kim Power	19	257	411	1794	858	1370	380	404	507	138	416	175	37	807	239	77
Nam Khat ($\text{N}\cdot\text{m}^{-1}\cdot\text{s}^{-1}$)	1131	2159	2072	865	844	995	707	1037	1500	1856	1056	1070				
Nam Kim Shear	12.0	69.3	91.5	269.5	159.2	225.6	93.0	91.4	110.5	44.8	90.6	50.5	18.2	139.8	66.2	30.0
Nam Khat ($\text{N}\cdot\text{m}^{-2}$)	370.4	530.6	520.7	302.1	294.6	348.2	261.9	337.4	422.9	531.9	363.2	355.5				
Nam Kim Velocity	1.8	3.8	4.6	6.8	5.4	8.5	4.1	4.6	5.0	3.2	4.8	3.7	2.5	6.7	4.5	2.8
Nam Khat ($\text{m}\cdot\text{s}^{-1}$)	3.8	4.5	4.8	3.9	3.8	3.4	3.1	3.9	3.7	3.6	3.0	3.1				

4.5. HEC-RAS Forecast Flood Stage and Discharge

Figure 11 provides the intercorrelations between the HEC-RAS discharge and stage fluctuations during the forecast time (3.5 and 5.5 days by GSM and HRM) in the Nam Kim (top graph) and in the Nam Khat (lower graph) channels at the outlets (RS101). The remarkable features were that the forecast Q and WL of the first rain (starting at 6 a.m. on 23 June 2011) corresponded well with hydrological gauged data, changing in WL proportionally well with the changes of flow values and the wrong predictions (marked by the red crosses and identified by means of a comparison with observed data in Nam Kim and the differences between GSM and HRM stage and flow in Nam Khat). Interestingly, when we compare the peaks of the two graphs, those of Nam Khat were intuitively not very natural (less smooth than expected) compared to the peaks of Nam Kim. This could be explained by the coarse temporal resolution of the forecast precipitation (6 h), which had stronger impacts on the

predicted Q and WL in the smaller watershed of Nam Khat than in the bigger one of Nam Kim. When it comes to FF prediction, the question of hydrological and meteorological uncertainty is well known and has often been discussed [12]. The agreements between the GSM- and HRM-based flows presented in Figure 11a were illustrated using the Nash–Sutcliffe efficiency (NSE) [34] for the predicted discharge of GSM and HRM rainfalls, which were 0.6 and 0.4, respectively. Based on the NSEs, using GSM precipitation appeared to perform better compared to using HRM, though satisfactory performances were observed for the first rain on 23 June 2011. On the other hand, there were some differences between forecasts and measured data for both cases on 26 June 2011 (red circle). In addition, by comparing the different uses of forecast rainfall, some false alarms and missing forecast (red crosses) likely could be seen on the graph. However, it is still difficult to conclude whether the uncertainties came from the hydrological models or from the rainfall models. We might need more calibrations for both rainfall models. The estimate accuracy could greatly benefit from rainfall data of higher quality [61]; possibly, rainfall from newer radar generations would be a good option. Unfortunately, there was no available on-site measured discharge and stage data for testing the forecast flow and stage for the Nam Khat reach.

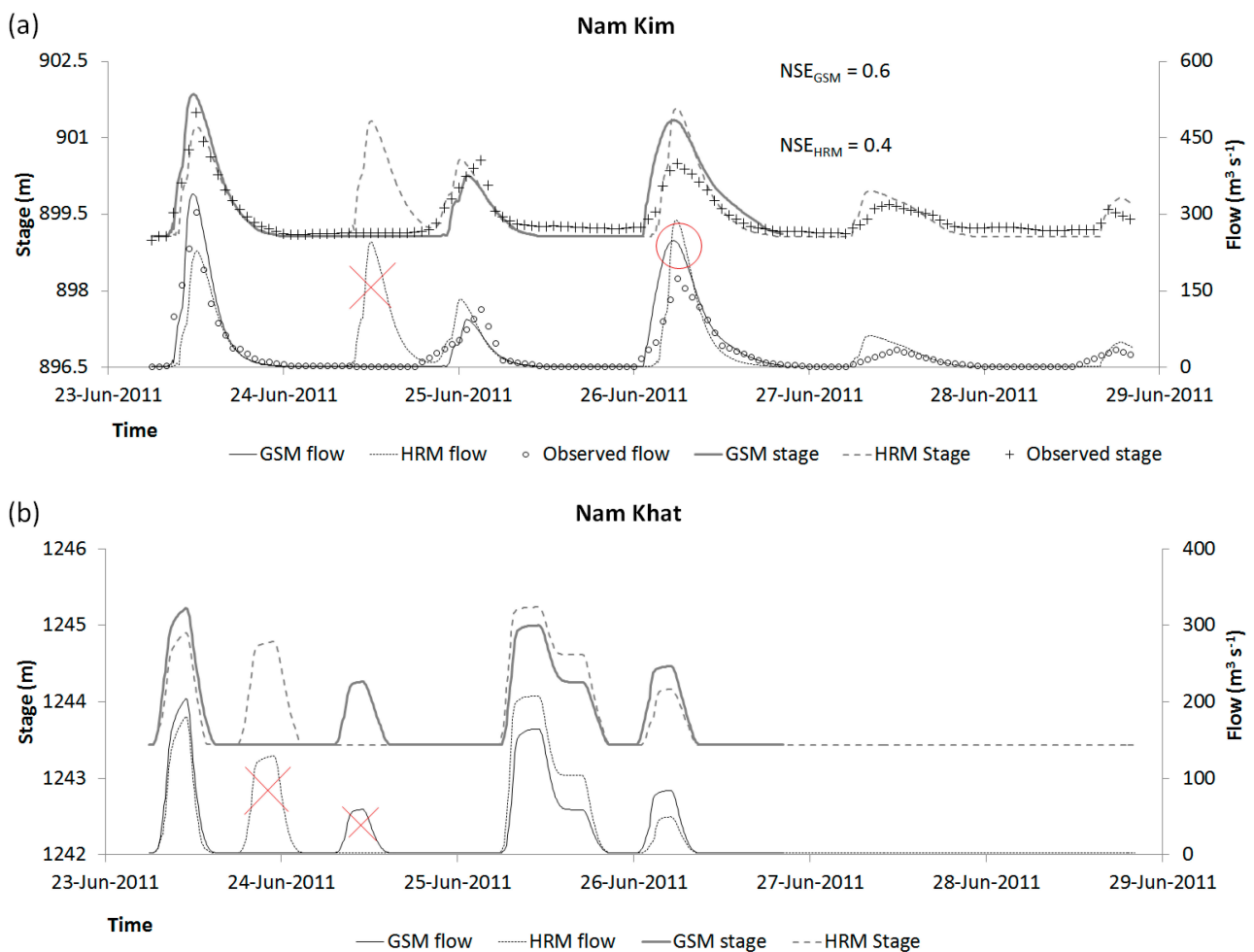


Figure 11. HEC-RAS forecast flow discharge and stages using observations at 6 a.m. 23 June 2011 of GSM and HRM. (a) for Nam Kim; and (b) for Nam Khat.

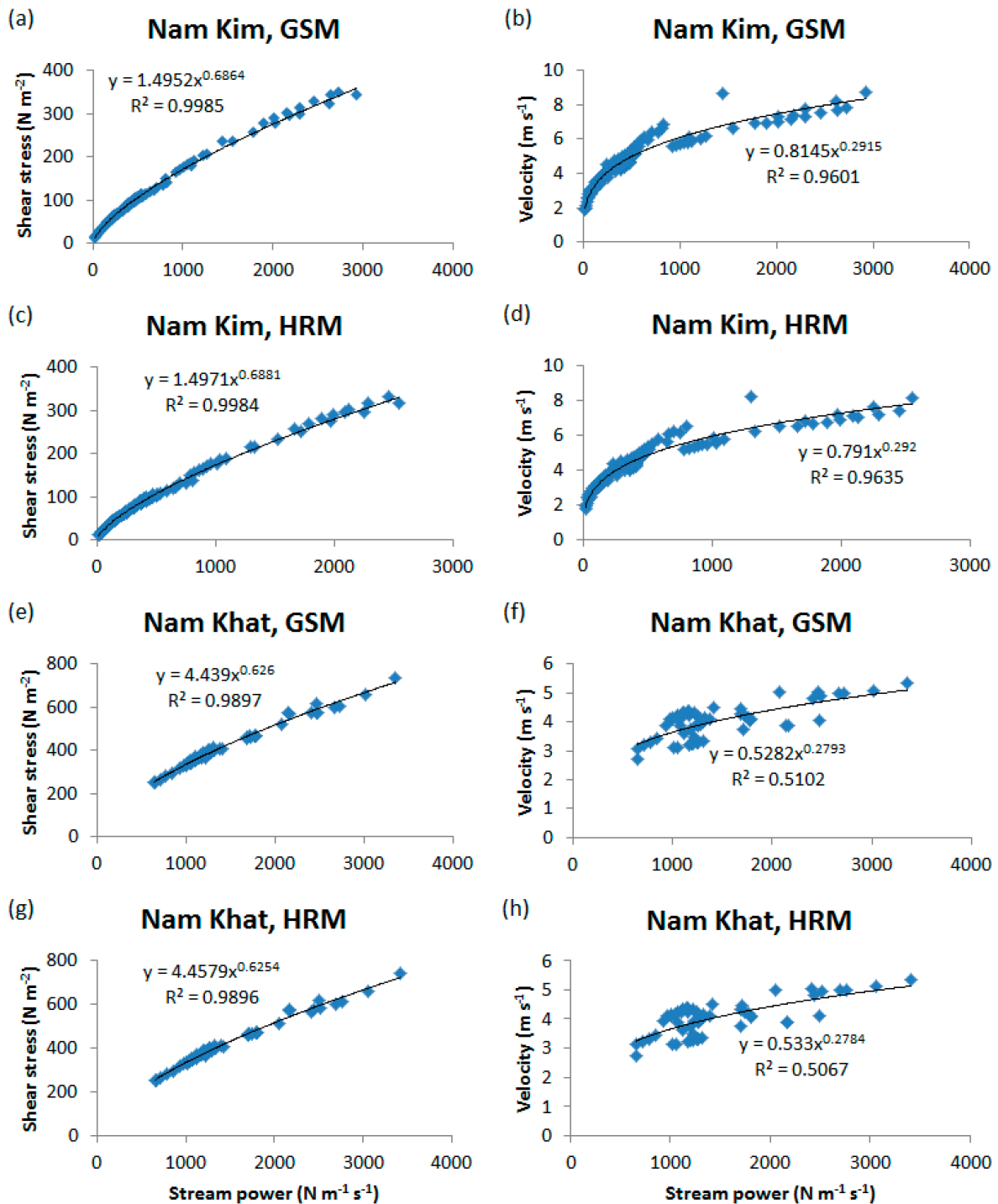


Figure 12. Forecasted stream power in the Nam Kim channel compared to. (a) Shear stress using the GSM rainfall; (b) velocity using the GSM rainfall; (c) shear stress employing the HRM rainfall; and (d) velocity using the HRM rainfall. Forecasted stream power in the Nam Khat channel compared to. (e) Shear stress employing the GSM rainfall; (f) velocity using the GSM rainfall; (g) shear stress using the HRM rainfall; and (h) velocity employing the HRM rainfall.

4.6. HEC-RAS Forecast Channel Velocity, Flow Power and Shearing Force

The total streamflow, shearing forces and velocity at individual RS (including interpolated RSs) were forecasted for 3.5 and 5.5 days using GSM and HRM rainfall, respectively, and the starting time of the forecast was at 6:00 on 23 June 2011. Furthermore, their relationships were presented by the power curves, equations and the regression squared values (R^2) (Figure 12). The shearing power varied greatly from 10 to 350 in Nam Kim using GSM precipitation (the peaks were a little lower compared to using HRM) and from about 220 to 750 $\text{N}\cdot\text{m}^{-2}$ in Nam Khat (for both GSM and HRM). Similarly, the flows were very powerful (ranging from 50 to 2500 in Nam Kim, from 650 to 3400 $\text{N}\cdot\text{m}^{-1}\cdot\text{s}^{-1}$), and there was not much difference between using GSM and HRM rainfall. The interesting point is that the strong correlations between streamflow power and shearing force were explicitly shown for all of the cases (all $R^2 \approx 0.99$; Figure 12a,c,e,g).

The mean streamflow speed was also predicted for all of the RSs of the two streams using GSM and HRM rainfall and scattered with the flow forces (Figure 12b,d,f,h). The flow speeds reached approximately $8 \text{ m}\cdot\text{s}^{-1}$ at some RSs in Nam Kim and about $5 \text{ m}\cdot\text{s}^{-1}$ in Nam Khat. Better velocity-stream power linkages were found with the prediction for Nam Kim ($R^2 \approx 0.96$), and there was less connection for Nam Khat ($R^2 \approx 0.51$). However, the FV values were more important when predicted at high speed and might exceed the FF threshold and cause flash flooding, as Vinet [13] asserted, namely that FFs are likely to occur when the flow velocities are several meters per second.

5. Summary and Conclusions

The findings of the study show that by coupling the two models, both the estimated water levels and discharge, using satellite and forecast rainfall by KINEROS2 and HEC-RAS agreed well with the field-measured data. The merits of the models were verified not only by the validations, but also by the precise, applicable outputs for FF prediction, such as peak discharge, flow stage, velocity and power. By using the GSM and HRM forecast rainfall, the models produced some errors in the prediction strategy. We assert that the models performed well, but the error source likely came from the forecast rainfall data. Therefore, we suggest an improvement in the accuracy of GSM and HRM production for the aim of providing an FF warning system with accurate rainfall. Although total time (about one hour) of the hydrological and NWP model calculations was still sufficient for providing timely forecasted Q, in the near future, it will be quickly improved due to the advancement of information technology. Additionally, combining the two models could accumulate errors from the models. Especially this problem is significant when the first model has large uncertainties. However, as hydrological models require various data sources for the inputs, this sources of uncertainty are important, as well.

We also found close relationships between river geometry (slope, top width and flow area) and hydrological responses and between those of hydraulic behavior (velocity, streamflow power and shearing forces). From the result analyses, we found reasonable outcomes for the ungauged watershed of Nam Khat using the so-called traditional concept of spatial proximity invented by [48]. This is meaningful for the enlargement of this approach to other poorly-gauged and ungauged watersheds in North Vietnam. Especially, FFs could occur in any watershed from small to large, even in

subwatersheds, and usually, not all watersheds are gauged. This approach of proximity was supported by some similar studies of Makungo *et al.* [53], Servat and Dezetter [66] and Boughton and Chiew [67].

Acknowledgments

We would like to acknowledge the Vietnam Natural Resources and Environment Corporation for providing us the topographical and geometric data and the Vietnam National Centre for Hydro-Meteorological Forecasting for supplying the meteorological data for this research. We also thank Geraldine Krause for her proofreading and the anonymous reviewers for their valuable comments.

Author Contributions

Hong Quang Nguyen was responsible for data analysis, writing the manuscript and communicating with the journal. Jan Degener and Martin Kappas were in charge of supervising the experiments, the structure of the paper and providing the main points for discussion in the Results and Introduction.

Conflicts of Interest

The authors declare no conflict of interest.

References

1. Ruiz-Villanueva, V.; Díez-Herrero, A.; Stoffel, M.; Bollschweiler, M.; Bodoque, J.M.; Ballesteros, J.A. Dendrogeomorphic analysis of flash floods in a small ungauged mountain catchment (Central Spain). *Geomorphology* **2010**, *118*, 383–392.
2. Zanon, F.; Borga, M.; Zoccatelli, D.; Marchi, L.; Gaume, E.; Bonnifait, L.; Delrieu, G. Hydrological analysis of a flash flood across a climatic and geologic gradient: The September 18, 2007 event in Western Slovenia. *J. Hydrol.* **2010**, *394*, 182–197.
3. Seo, D.; Lakhankar, T.; Mejia, J.; Cosgrove, B.; Khanbilvardi, R. Evaluation of Operational National Weather Service Gridded Flash Flood Guidance Over the Arkansas Red River Basin. *JAWRA* **2012**, doi:10.1111/jawr.12087.
4. Masoud, A.A. Runoff modeling of the wadi systems for estimating flash flood and groundwater recharge potential in Southern Sinai, Egypt. *Arab. J. Geosci.* **2011**, *4*, 785–801.
5. Rozalis, S.; Morin, E.; Yair, Y.; Price, C. Flash flood prediction using an uncalibrated hydrological model and radar rainfall data in a Mediterranean watershed under changing hydrological conditions. *J. Hydrol.* **2010**, *394*, 245–255.
6. Vietnam Assessment Report on Climate Change (VARCC) . Available online: http://www.unep.org/pdf/dtie/VTN_ASS_REP_CC.pdf (accessed on 16 November 2015).
7. Tao, J.; Barros, A.P. Prospects for flash flood forecasting in mountainous regions—An investigation of Tropical Storm Fay in the Southern Appalachians. *J. Hydrol.* **2013**, *506*, 69–89.
8. Naulin, J.P.; Payrastre, O.; Gaume, E. Spatially distributed flood forecasting in flash flood prone areas: Application to road network supervision in Southern France. *J. Hydrol.* **2013**, *486*, 88–99.

9. Villarini, G.; Krajewski, W.F.; Ntelekos, A.A.; Georgakakos, K.; Smith, J.A. Towards probabilistic forecasting of flash floods: The combined effects of uncertainty in radar-rainfall and flash flood guidance. *J. Hydrol.* **2010**, *394*, 275–284.
10. Committee to Assess NEXRAD Flash Flood Forecasting Capabilities at Sulphur Mountain, California; Board on Atmospheric Sciences and Climate; Division on Earth and Life Studies; National Research Council. *Flash Flood Forecasting over Complex Terrain: With an Assessment of the Sulphur Mountain NEXRAD in Southern California*; The National Academies Press: Washington, DC, USA, 2005.
11. Vincendon, B.; Ducrocq, V.; Dierer, S.; Kotroni, V.; Le Lay, M.; Milelli, M.; Quesney, A.; Saulnier, G.M.; Rabuffetti, D.; Bouilloud, L.; *et al.* Flash flood forecasting within the PREVIEW project: Value of high-resolution hydrometeorological coupled forecast. *Meteorol. Atmos. Phys.* **2009**, *103*, 115–125.
12. Montz, B.E.; Grunfest, E. Flash flood mitigation: Recommendations for research and applications. *Glob. Environ. Chang. B Environ. Hazards* **2002**, *4*, 15–22.
13. Vinet, F. Geographical analysis of damage due to flash floods in southern France: The cases of 12–13 November 1999 and 8–9 September 2002. *Appl. Geogr.* **2008**, *28*, 323–336.
14. Yates, D.N.; Warner, T.T.; Leavesley, G.H. Prediction of a flash flood in complex terrain. Part II: A comparison of flood discharge simulations using rainfall input from radar, a dynamic model, and an automated algorithmic system. *J. Appl. Meteorol.* **2000**, *39*, 815–825.
15. Abderrezzak, K.E.; Paquier, A.; Mignot, E. Modelling flash flood propagation in urban areas using a two-dimensional numerical model. *Nat. Hazards* **2009**, *50*, 433–460.
16. Volkmann, T.H.M.; Lyon, S.W.; Gupta, H.V.; Troch, P.A. Multicriteria design of rain gauge networks for flash flood prediction in semiarid catchments with complex terrain. *Water Resour. Res.* **2010**, *46*, W11554.
17. Snell, S. *A Flash Flood Prediction Model for Rural and Urban Basins in New Mexico*; WRRI Technical Completion Report; New Mexico Water Resources Research Institute: Las Cruces, NM, USA, 2002.
18. Javelle, P.; Fouchier, C.; Arnaud, P.; Lavabre, J. Flash flood warning at ungauged locations using radar rainfall and antecedent soil moisture estimations. *J. Hydrol.* **2010**, *394*, 267–274.
19. Reed, S.; Schaake, J.; Zhang, Z.Y. A distributed hydrologic model and threshold frequency-based method for flash flood forecasting at ungauged locations. *J. Hydrol.* **2007**, *337*, 402–420.
20. Norbiato, D.; Borga, M.; Dinale, R. Flash flood warning in ungauged basins by use of the flash flood guidance and model-based runoff thresholds. *Meteorol. Appl.* **2009**, *16*, 65–75.
21. Liu, W.C.; Wu, C.Y. Flash flood routing modeling for levee-breaks and overbank flows due to typhoon events in a complicated river system. *Nat. Hazards* **2011**, *58*, 1057–1076.
22. Unkrich, C.L. Real-time Flash Flood Forecasting Using Weather Radar and Distributed Rainfall-Runoff Model. In Proceedings of the 2nd Joint Federal Interagency Conference, Las Vegas, NV, USA, 27 June–1 July 2010.
23. Morin, E.; Jacoby, Y.; Navon, S.; Bet-Halachmi, E. Towards flash-flood prediction in the dry Dead Sea region utilizing radar rainfall information. *Adv. Water Resour.* **2009**, *32*, 1066–1076.
24. Younis, J.; Anquetin, S.; Thielen, J. The benefit of high-resolution operational weather forecasts for flash flood warning. *Hydrol. Earth Syst. Sci.* **2008**, *12*, 1039–1051.

25. Wardah, T.; Abu Bakar, S.H.; Bárdossy, A.; Maznorizan, M. Use of geostationary meteorological satellite images in convective rain estimation for flash-flood forecasting. *J. Hydrol.* **2008**, *356*, 283–298.
26. Youssef, A.M.; Pradhan, B.; Hassan, A.M. Flash flood risk estimation along the St. Katherine road, southern Sinai, Egypt using GIS based morphometry and satellite imagery. *Environ. Earth Sci.* **2011**, *62*, 611–623.
27. Borga, M.; Stoffel, M.; Marchi, L.; Marra, F.; Jakob, M. Hydrogeomorphic response to extreme rainfall in headwater systems: Flash floods and debris flows. *J. Hydrol.* **2014**, *518*, 194–205.
28. Krzysztofowicz, R. Probabilistic flood forecast: Exact and approximate predictive distributions. *J. Hydrol.* **2014**, *517*, 643–651.
29. Georgakakos, K.P. On the design of national, real-time warning systems with capability for site-specific, flash-flood forecasts. *Bull. Am. Meteorol. Soc.* **1986**, *67*, 1233–1239.
30. Ntelekos, A.A.; Georgakakos, K.P.; Krajewski, W.F. On the Uncertainties of Flash Flood Guidance: Toward Probabilistic Forecasting of Flash Floods. *J. Hydrometeorol.* **2006**, *7*, 896–915.
31. Estupina-Borrell, V.; Dartus, D.; Ababou, R. Flash flood modeling with the MARINE hydrological distributed model. *Hydrol. Earth Syst. Sci.* **2006**, *3*, 3397–3438.
32. Quintero, F.; Sempere-Torres, D.; Berenguer, M.; Baltas, E. A scenario-incorporating analysis of the propagation of uncertainty to flash flood simulations. *J. Hydrol.* **2012**, *460*, 90–102.
33. Yatheendradas, S.; Wagener, T.; Gupta, H.; Unkrich, C.; Goodrich, D.; Schaffner, M.; Stewart, A. Understanding uncertainty in distributed flash flood forecasting for semiarid regions. *Water Resour. Res.* **2008**, doi:10.1029/2007WR005940.
34. Nash, J.E.; Sutcliffe, J.V. River flow forecasting through conceptual models 1: A discussion of principles. *J. Hydrol.* **1970**, *10*, 282–290.
35. Mudd, S.M. Investigation of the hydrodynamics of flash floods in ephemeral channels: Scaling analysis and simulation using a shock-capturing flow model incorporating the effects of transmission losses. *J. Hydrol.* **2006**, *324*, 65–79.
36. Gupta, H. *Development of a Site-Specific Flash Flood Forecasting Model for the Western Region*; Final Report for COMET Proposal Entitled; University of Arizona: Tucson, AZ, USA, 2006.
37. U.S. Department of Commerce. *Advanced Hydrologic Prediction Services—Concept of Services and Operations*; U.S. Department of Commerce: Washington, DC, USA, 2002.
38. Kourgialas, N.N.; Karatzas, G.P.; Nikolaidis, N.P. Development of a thresholds approach for real-time flash flood prediction in complex geomorphological river basins. *Hydrol. Process.* **2012**, *26*, 1478–1494.
39. Anh, P.T.Q.; Gomi, T.; MacDonald, L.H.; Mizugaki, S.; Khoa, P.V.; Furuichi, T. Linkages among land use, macronutrient levels, and soil erosion in northern Vietnam: A plot-scale study. *Geoderma* **2014**, *232–234*, 352–362.
40. Ranzi, R.; Le, T.H.; Rulli, M.C. A RUSLE approach to model suspended sediment load in the Lo river (Vietnam): Effects of reservoirs and land use changes. *J. Hydrol.* **2012**, *422–423*, 17–29.
41. Smith, R.E.; Goodrich, D.; Woolhiser, D.A.; Unkrich, C.L. KINEROS—A kinematic runoff and erosion model. In *Computer Models of Watershed Hydrology*; Singh, V.P., Ed.; Water Resources Publications: Highlands Ranch, CO, USA, 1995; p. 1130.

42. Smith, R.E.; Goodrich, D.C.; Unkrich, C.L. Simulation of selected events on the Catsop catchment by KINEROS2: A report for the GCTE conference on catchment scale erosion models. *Catena* **1999**, *37*, 457–475.
43. Woolhiser, D.A.; Smith, R.E.; Goodrich, D.C. *KINEROS: A Kinematic Runoff and Erosion Model: Documentation and User Manual*; ARS-77; Agricultural Research Service (ARS): Washington, DC, USA, 1990.
44. Brunner, G.W.; United States Army Corps of Engineers; Institute for Water Resources (U.S.); Hydrologic Engineering Center (U.S.). *HEC-RAS River Analysis System: Hydraulic Reference Manual, Version 4.1 January 2010*; US Army Corps of Engineers: Davis, CA, USA, 2010.
45. Horritt, M.S.; Bates, P.D. Evaluation of 1D and 2D numerical models for predicting river flood inundation. *J. Hydrol.* **2002**, *268*, 87–99.
46. Shames, I.H. *Mechanics of Fluids*; McGraw-Hill Book Company: New York, NY, USA, 1962.
47. Brunner, G.W.; United States Army Corps of Engineers; Institute for Water Resources (U.S.); Hydrologic Engineering Center (U.S.). *HEC-RAS, River Analysis System: Hydraulic Reference Manual, Version 3.1 November 2002*; US Army Corps of Engineers: Davis, CA, USA, 2002.
48. Blöschl, G. Rainfall–runoff modelling of ungauged catchments. In *Encyclopedia of Hydrological Sciences*; Anderson, M.G.E., Ed.; John Wiley & Sons: Chichester, UK, 2005; pp. 2061–2080.
49. Krishnamurti, T.N.; Bedi, H.S.; Hardiker, V.M.; Ramaswamy, L. *An Introduction to Global Spectral Modeling*, 2nd ed.; Atmospheric and Oceanographic Sciences Library; Springer: Berlin, Germany, 2006.
50. Majewski, D. HRM—User’s Guide for the HRM with the SSO Scheme; Vrs. 2.5 and Higher; Deutscher Wetterdienst, Press and Public Relations: Offenbach, Germany, 2009.
51. Centre for Resources and Environment, National Institute of Agricultural Planning and Projection (NIAPP). *Yen Bai Soil Map Report*; NIAPP: Hanoi, Vietnam, 1996.
52. Vietnam National Centre for Hydro-Meteorological Forecasting (NCHMF). Available online: <http://www.nchmf.gov.vn/web/vi-VN/71/29/45/Default.aspx> (accessed on 7 March 2014).
53. Makungo, R.; Odiyo, J.O.; Ndiritu, J.G.; Mwaka, B. Rainfall–runoff modelling approach for ungauged catchments: A case study of Nzhelele River sub-quaternary catchment. *Phys. Chem. Earth* **2010**, *35*, 596–607.
54. Marchi, L.; Borga, M.; Preciso, E.; Gaume, E. Characterisation of selected extreme flash floods in Europe and implications for flood risk management. *J. Hydrol.* **2010**, *394*, 118–133.
55. Lumbroso, D.; Gaume, E. Reducing the uncertainty in indirect estimates of extreme flash flood discharges. *J. Hydrol.* **2012**, *414–415*, 16–30.
56. Rodriguez, L.B.; Cello, P.A.; Vionnet, C.A.; Goodrich, D. Fully conservative coupling of HEC-RAS with MODFLOW to simulate stream–aquifer interactions in a drainage basin. *J. Hydrol.* **2008**, *353*, 129–142.
57. Klimes, J.; Benešová, M.; Vilímek, V.; Bouška, P.; Rapre, A.C. The reconstruction of a glacial lake outburst flood using HEC-RAS and its significance for future hazard assessments: An example from Lake 513 in the Cordillera Blanca, Peru. *Nat. Hazards* **2014**, *71*, 1617–1638.
58. Sarhadi, A.; Soltani, S.; Modarres, R. Probabilistic flood inundation mapping of ungauged rivers: Linking GIS techniques and frequency analysis. *J. Hydrol.* **2012**, *458–459*, 68–86.

59. Versini, P.A. Use of radar rainfall estimates and forecasts to prevent flash flood in real time by using a road inundation warning system. *J. Hydrol.* **2012**, *416*, 157–170.
60. Pekarova, P.; Svoboda, A.; Miklánek, P.; Škoda, P.; Halmová, D.; Pekár, J. Estimating Flash Flood Peak Discharge in Gidra and Parna Basin: Case Study for the 7–8 June 2011 Flood. *J. Hydrol. Hydromech.* **2012**, *60*, 206–216.
61. Looper, J.P.; Vieux, B.E. An assessment of distributed flash flood forecasting accuracy using radar and rain gauge input for a physics-based distributed hydrologic model. *J. Hydrol.* **2012**, *412*, 114–132.
62. Alfieri, L.; Thielen, J.; Pappenberger, F. Ensemble hydro-meteorological simulation for flash flood early detection in southern Switzerland. *J. Hydrol.* **2012**, *424*, 143–153.
63. Carpenter, T.M.; Sperflage, J.A.; Georgakakos, K.P.; Sweeney, T.; Fread, D.L. National threshold runoff estimation utilizing GIS in support of operational flash flood warning systems. *J. Hydrol.* **1999**, *224*, 21–44.
64. Ancona, M.; Corradi, N.; Dellacasa, A.; Delzanno, G.; Dugelay, J.L.; Federici, B.; Gourbesville, P.; Guerrini, G.; la Camera, A.; Rosso, P.; *et al.* On the Design of an Intelligent Sensor Network for Flash Flood Monitoring, Diagnosis and Management in Urban Areas Position Paper. *Procedia Comput. Sci.* **2014**, *32*, 941–946.
65. El-Magd, I.A.; Hermas, E.; Bastawesy, M.E. GIS-modelling of the spatial variability of flash flood hazard in Abu Dabbab catchment, Red Sea Region, Egypt. *Egypt. J. Remote Sens. Space Sci.* **2010**, *13*, 81–88.
66. Servat, E.; Dezetter, A. Rainfall-runoff modelling and water resources assessment in northwestern Ivory Coast. Tentative extension to ungauged catchments. *J. Hydrol.* **1993**, *148*, 231–248.
67. Boughton, W.; Chiew, F. Estimating runoff in ungauged catchments from rainfall, PET and the AWBM model. *Environ. Model. Softw.* **2007**, *22*, 476–487.

© 2015 by the authors; licensee MDPI, Basel, Switzerland. This article is an open access article distributed under the terms and conditions of the Creative Commons Attribution license (<http://creativecommons.org/licenses/by/4.0/>).